Localised corrosion of heat treated alloys Part 1 – repassivation potential of alloy 600 as function of solution chemistry and thermal aging

G. Tormoen*[1], N. Sridhar[2] and A. Anderko[3]

The crevice repassivation potential E_{rcrev} of alloy 600 was measured as a function of chloride concentration, inhibitor concentration, temperature and degree of sensitisation (DOS) due to thermal aging. Electrochemical potentiokinetic reactivation tests were performed on thermally aged alloy 600 to correlate the DOS with E_{rcrev} results. The electrochemical potentiokinetic reactivation results agreed well with the literature, and differed in the apparent sensitisation kinetics from E_{rcrev}. The crevice repassivation potential was found to be inversely related to test temperature, chloride concentration, and DOS due to thermally aging the material. Additions of nitrate were found to significantly elevate the repassivation potential of both annealed and sensitised material. The results form the basis for establishing a model to predict the occurrence of localised corrosion for in service, real world materials used in the processing industry.

Keywords: Localised corrosion, Alloy 600, Repassivation potential, Thermal aging

Introduction

Characterising thermal instabilities, instigated during fabrication processes, in nominally corrosion resistant alloys and their effects on corrosion behaviour is crucial to predicting the life expectancies of these materials in real world applications.[1] This is true for alloy 600 (UNS N06600), a nominally corrosion resistant alloy used primarily in nuclear steam generators and chemical processing plants. Like other Fe–Ni–Cr alloys, alloy 600 undergoes precipitation of chromium carbides at grain boundaries when subjected to elevated temperatures[2] (500–900°C) that can be achieved during fabrication processes. The precipitation is initially accompanied by a chromium depleted grain boundary layer (GBCD), owing to the different diffusivities of carbon and chromium in the austenite matrix. The chromium depletion broadens spatially with time at temperatures in the precipitation regime until the carbon activity in the carbides is equal to that in the surrounding matrix. The time required to achieve this is dependent on the carbon content of the material, but typically occurs within a day at 700°C.[3–6] Continued thermal exposure results in the 'healing' of the chromium depleted layer, which returns the chromium concentration of the chromium depleted layer to that of the bulk matrix.

Processing infrastructure must undergo some fabrication processes, but healing of fabricated structures is not feasible. Therefore, materials may be placed in service with some degree of sensitisation (DOS). The chromium concentration in the depleted region has been found to drop to 3%,[5] which is well below the 9·8–11·7% criterion for establishing passivity in these alloys.[7] This loss of local passivity adversely impacts the general corrosion and stress corrosion cracking resistance of these alloys. Sensitisation may also be detrimental to localised corrosion resistance, as pits may easily initiate in the depleted regions generating harsh local chemistries in and around the pit which eventually propagate into the non-depleted regions. However, detailed investigation of the effect of such sensitisation on localised corrosion (pitting, crevice corrosion) has not been reported for this alloy. Unlike the case of general corrosion, where the alloy is passive in regions devoid of chromium depletion, under localised corrosion conditions, the non-depleted passive film can be destabilised as well. Therefore, the presence of Cr depleted grain boundaries adds another layer of complexity to the local destabilisation of the passive film in a localised corrosion environment. The objective of this study is to evaluate the effect of sensitisation on crevice and pitting corrosion resistance of alloy 600.

Background

Alloy 600 sensitisation

Sensitisation in alloy 600 is a consequence of grain boundary carbide formation. The carbon solubility limit

[1]Southwest Research Institute, Department of Materials Engineering, 6220 Culebra Road, San Antonio, TX 78238, USA
[2]Det Norske Veritas, 5777 Frantz Road, Dublin, OH 43017, USA
[3]OLI Systems Inc., 108 American Road, Morris Plains, NJ 07950, USA

*Corresponding author, email garth.tormoen@swri.org

Published by Maney on behalf of the Institute
Received 20 December 2007; accepted 9 June 2008
DOI 10.1179/147842208X320315

in this alloy approximately scales with temperature as shown in equation (1) (Ref. 8)

$$\%\text{carbon} = e^{\left(\frac{T-1445}{128}\right)} \quad (1)$$

At 1150°C, the solubility is ~0·1%, while at 650°C, the solubility is reduced to ~0·002%. Carbon is invariably present as an impurity in commercially produced alloy 600. The commercially produced alloy is typically thermomechanically processed and mill annealed at 1010°C. This treatment results in relatively precipitate free grain boundaries, but some matrix carbides remain to minimise grain growth. A high temperature solution annealing (at 1100°C) is sometimes carried out in the laboratory to ensure complete dissolution of all carbides before controlled aging studies. Grain boundary carbide precipitation occurs when a mill or solution annealed alloy is heated or cooled slowly through a temperature range of 500 to 900°C. The composition of carbides in alloy 600 has been determined to be Cr_7C_3.[8]

Sensitisation occurs because the carbide is in equilibrium with the carbon and chromium in the grain boundary as shown in equation (2)

$$7Cr + 3C \rightleftharpoons Cr_7C_3; K = \frac{a_{Cr_7C_3}}{\left(a_{Cr_7}\right)^7 \times (a_C)^3} \quad (2)$$

The activity of the carbide can be regarded as unity, leaving the activity of the carbon at the grain boundary to be inversely related to the activity of chromium. Thus, at initial stages of precipitation, the carbon activity is high and the chromium activity is low. Because carbon diffusivity is sufficiently high, the carbon activity will attain rapid equilibrium with the carbide in the bulk of the grain. However, the chromium is less mobile and therefore diffusion from the interior of the grain lags that of the carbon. This results in a chromium depleted layer near the precipitated carbide/grain boundary. As the corrosion resistance of this alloy is largely due to the chromium content, the chromium depleted layer is susceptible to corrosion, resulting in intergranular attack, a phenomenon termed sensitisation.

The first direct evidence of grain boundary chromium depletion in alloy 600 was reported by Was *et al.*,[5] who found that the depth of depletion (i.e. the difference between the lowest chromium content in the depleted zone and the bulk/matrix chromium content) increased for aging times up to 10 h at 700°C. Continued aging at 700°C resulted in healing of the GBCD, although complete recovery was not evident before 100 h aging. Other studies examined the kinetics for 'full' sensitisation (minimum Cr concentration in GBCD) of alloy 600 as well, and these findings are sorted by carbon content and summarised in Table 1.

Table 1 Selected sensitisation kinetics data from literature

C content	Hours at 700°C to minimum Cr	Reference
0·023	17	4
0·032	10	5
0·043	7	4
0·05	5	6
0·054	5	4
0·093	2	3

Heat to heat variations in the carbon content can dramatically alter the sensitisation kinetics for alloy 600. Quantitative modelling of the sensitisation process has been well understood for simple alloy systems such as alloy 600.[7–11] In particular, there exists a substantial body of work regarding the effects of grain boundary precipitation on stress corrosion cracking of alloy 600,[9–22] as cracking of nuclear steam generator piping accounts for a significant portion of all material failures for these systems.[23] Conversely, work performed to delineate sensitisation effects on the occurrence of intergranular corrosion have focused on accelerated test techniques[2,6–8,11,17,18,24] that directly exploit the effect of microchemical segregations of the alloy on corrosion in severely oxidising, acidic environments or on the electrochemical polarisation behaviour. In the latter case, a standard test method, called the electrochemical potentiokinetic reactivation (EPR) test, is used to characterise the degree of passive film stability in an acidic environment that exhibits active–passive behaviour. While these tests allow identification of improvements in alloying and heat treatment, and serve as good quality control tools, the generated data does not necessarily allow one to predict the performance lifetime of these materials in real world environments. Furthermore, these tests do not address localised corrosion susceptibility of the alloy. The oxidising, acid environments, such as the ASTM A 262 test,[25] do not cause pitting or crevice corrosion. The EPR test is typically performed in dilute sulphuric acid and accesses the potentials in the active–passive regime. Nevertheless, the EPR test results could be used as a simple measure of the DOS to correlate localised corrosion susceptibility determined in environments that cause localised corrosion.

Repassivation potential as predictor for service lifetime

The purpose of this study was to generate thermal aging dependent localised corrosion parameters in the laboratory for use in a model to predict the localised corrosion susceptibility of alloy 600 subjected to fabrication procedures and placed in service in any 'real world' environments. For this, the crevice repassivation potential E_{rcrev} was selected as the threshold parameter, based upon previous work showing its sensitivity to microstructure and applicability for predicting the lifetime expectancy of candidate high level nuclear waste container materials. The authors' previous work,[26,27] has also shown that the repassivation potential generated for a limited set of environments could be used to predict the values for a much wider set of environments containing aggressive, inhibitive, and diluent species. To study the effect of heat treatment on localised corrosion, the following methodology was used:

(i) measure E_{rcrev} in aqueous chloride environments solely as a function of metallurgical differences (microstructural evolution due to thermal aging), and correlate the results with DOS derived from EPR tests
(ii) derive parameters for modelling the effect of metallurgy and alloying content on E_{rcrev}
(iii) measure the effects of inhibitors on E_{rcrev} independent of metallurgical variations (solution annealed condition only)

(iv) derive parameters to model the effect of inhibitors as a function of alloy composition
(v) integrate these parameters in order to predict the effect of inhibitors and microstructure on E_{rcrev}
(vi) test the resulting model by comparing measured with predicted E_{rcrev} values for aged specimens in the absence and in the presence of inhibitor ions.

This paper deals with the first topic. The topics (iii) and (iv) were studied in detail in a recent paper.[28] The topics (ii), (v), and (vi) will be the subject of a forthcoming companion paper.[29]

Experimental

Materials

Specimens of alloy 600 were obtained from two different heats (arbitrarily referred to as lots 1 and 2) in the mill annealed condition from Metal Samples Co. (Munford, AL, USA) with the compositions shown in Table 2. Some specimens were tested in the mill annealed condition, while the others were solution annealed at 1100°C for 30 min in a Lindberg model no. 51333 furnace. Solution annealed specimens were then subjected to thermal aging treatments at 700°C for times up to 168 h. Upon reaching the specified thermal aging or solution annealing time, specimens were immediately quenched to room temperature in an agitated water bath.

All specimens were polished on a Si–C grinding wheel in sequence from 60 to 600 grit, and subsequently degreased in a 10-minute ultrasonic acetone bath. The crevices were created by attaching serrated polytetrafluoroethylene washers (12 teeth per side) to each side of the specimen using C-276 bolts isolated through polytetrafluoroethylene sleeves and an initial torque of 0·14 N m (20 in oz). Each crevice site (tooth) consists of an area of 0·06 cm^2. The specimens were attached to a sample holder machined out of C-276 in order to establish the electrical connection outside the cell. An image of a specimen with crevice formers attached is shown in Fig. 1. Immersion into test solutions occurred within one hour of degreasing.

Electrochemical potentiokinetic reactivation test

The EPR scans were performed following the protocol outlined in ASTM G 108.[30] First, solutions were prepared by adding 9·7 mg KSCN (Fischer Scientific) and 9·8 g H_2SO_4 (Fischer Scientific) to 2 L of magnetically stirred deionised water (Ω=17 to 18 MΩ cm). Next, samples were affixed in either a 350 mL Avesta cell or immersed in a 1 L glass kettle, and approximately 250 or 600 mL of test solution added to the cell respectively. Then, the cells were deaerated by purging with grade 5·0 nitrogen (airgas) for 30 min before testing.

The EPR test involved a potential sweep from 150 mV below open circuit potential to 400 mV versus saturated calomel electrode (SCE), immediately followed by a reverse sweep to the initial potential at a rate of 0·167 mV s^{-1}. The corrosion current is recorded during the potential sweep, and a potential versus current plot is created. The maximum current recorded in the reverse scan is then normalised by the maximum current in the forward scan to yield the anodic peak ratio (APR), which is used to quantify the DOS.[31]

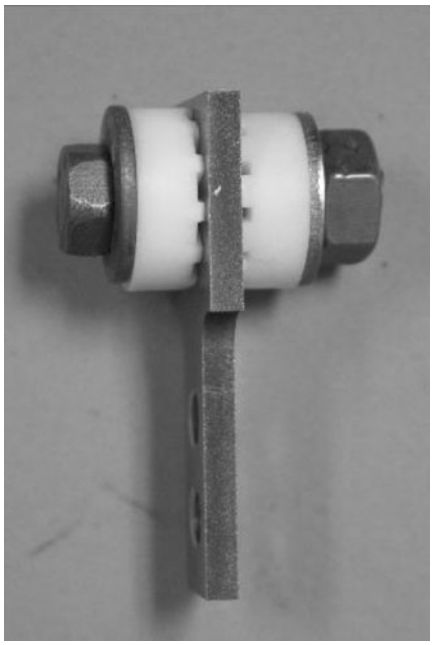

1 Image of test specimen with crevice formers attached

Crevice repassivation potential tests

Crevice repassivation potential E_{rcrev} measurements were recorded from scans made following the cyclic potentiodynamic polarisation (CPP) and the potential staircase (PS) methods. Solutions were prepared by adding: 0·012, 0·059, 0·12, 0·59 or 4·69 g NaCl (Fischer Scientific) to 2 L deionised water (Ω=17 to 18 MΩ cm) to yield: 10^{-4}, 5×10^{-4}, 10^{-3}, 5×10^{-3} or 0·04M solutions respectively. For the examination of the effects of nitrate inhibitor ions, 6·8 or 68 g $NaNO_3$ (Fischer Scientific) were added to the above solutions to introduce 0·04 or 0·4M NO_3^- respectively. Before testing, test cells were deaerated by purging with grade 5·0 nitrogen (airgas) for a minimum of 1 h. Cells were heated to and maintained at 60°C by inserting into a thermostatically controlled heater that continuously monitored the temperature of the test solution.

Cyclic potentiodynamic polarisation scans were performed by scanning the working electrode potential from open circuit potential to +1 V versus SCE at a rate of 0·167 mV s^{-1}, immediately followed by a reverse scan at the same rate to −400 mV versus SCE. Potential staircase scans raised the working electrode potential to a specified value (400–500 mV versus SCE) and held that potential for up to four days. The potential was then

Table 2 Alloy 600 major element compositions, wt-%

UNS	Mill	Fe	Ni	Cr	Mn	Ti	C	Al	Cu
N06600	Huntington	9·69	75·09	14·66	0·28	<0·310	0·02	<0·172	0·2
N06600	Huntington	9·19	74·41	15·56	0·21	0·23	0·04	0·252	0·04

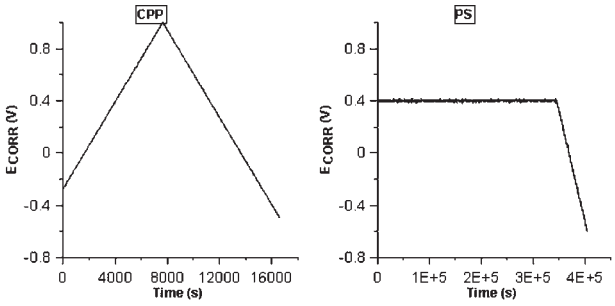

2 Potential (SCE) versus time plots for two repassivation test methods used

scanned in the reverse direction at a rate of $-0{\cdot}0167$ mV s^{-1} to a final potential of -400 mV versus SCE. Both techniques were also programmed with 'current triggers', which would automatically reverse the potential scan if a charge density of 10 C cm^{-3} (31·5 mA h, assuming overall crevice area) was achieved. E_{rcrev} was recorded for both techniques as the highest potential that corresponded to a current density of <1 μA cm^{-2} when scanned in the reverse direction.

To illustrate the differences between the CPP and PS techniques, Fig. 2 tracks the potential and current from actual tests performed with each technique.

Cyclic potentiodynamic polarisation imposes a higher overall potential on the corrosion specimen, to the point where transpassive dissolution of Cr or water breakdown may occur possibly affecting the composition of the passive film as well as the recorded current. Potential staircase holds the specimen at a less elevated potential, but for substantially longer periods of time. Cyclic potentiodynamic polarisation tests may scan potential too quickly, and developed pits may therefore not grow deep enough to yield a repassivation potential independent of charge density. The PS method is time consuming, and for nominally corrosion resistant alloys, the 400 mV (SCE) hold may not surpass the alloys' repassivation potential, and no localised corrosion may develop. Therefore, recorded data were validated by observing if PS showed evidence of pitting during the potentiostatic polarisation through a fluctuating current response, and for both protocols by examining the specimen after the test and looking for signs of localised corrosion. If these criteria were not met, the test results were not included in the analysis.

Experimentally determined E_{rcrev} are reported as single value data. However, the reproducibility of E_{rcrev} data depends on the chloride concentration, or more generally, the aggressiveness of the solution and test parameters, such as the crevice tightness and total

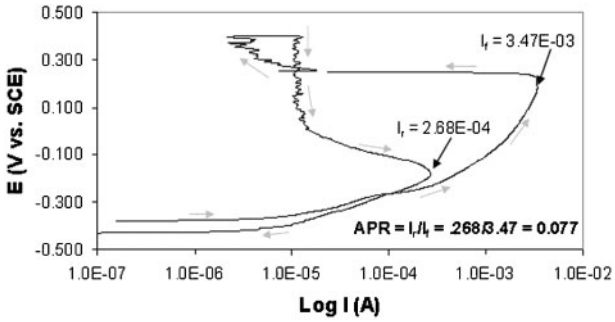

3 Representative EPR results used to determine APR

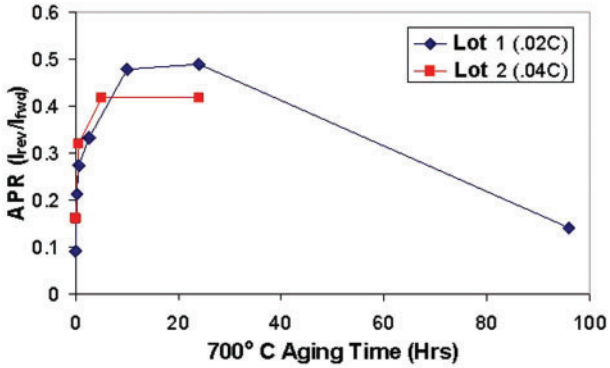

4 Anodic peak ratios recorded in 0·05M H_2SO_4 + 5E-5M KSCN for alloy 600 heats that were solution annealed and subsequently subjected to thermal aging treatments at 700°C for times shown

charge passed. For CPP tests, the E_{rcrev} value has been shown to have an error of about ± 40 mV.[32–34] For PS tests, the dispersion has been somewhat less, ranging from ± 10 to ± 20 mV, depending on the chloride concentration,[28] and the values reported herein should be considered accordingly.

Results

Electrochemical potentiokinetic reactivation tests

Initial EPR tests using the standard 0·5M H_2SO_4 solution were found to be too aggressive to discern DOS for different thermal treatments of alloy 600. A more dilute test solution of 0·05M $H_2SO_4 + 5 \times 10^{-5}$M KSCN was found to adequately distinguish between levels of sensitisation for alloy 600 in the mill annealed and solution annealed state, and was therefore implemented for the thermally aged specimens. A representative example of the E versus log I curve from the EPR test is shown in Fig. 3, with the APR labelling method displayed on the plot.

Following this procedure, APRs from solution annealed specimens aged up to 24 h at 700°C are shown in Fig. 4.

Tests demonstrated that the level of sensitisation increases with aging times between 10 and 24 h for lot 1 and to 5 h for lot 2. Healing, or a return of the APR to solution annealed values, was observed after 96 h for lot 1. The literature data on the time required for the lowest chromium content in the depletion zone for alloy 600 sensitisation shown previously in Table 1 are displayed graphically in Fig. 5.

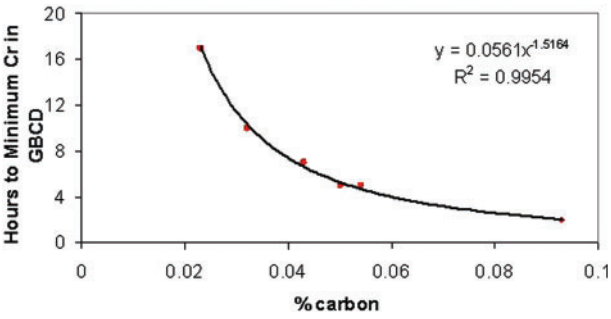

5 Trend of carbon content with time to achieve full or maximum sensitisation

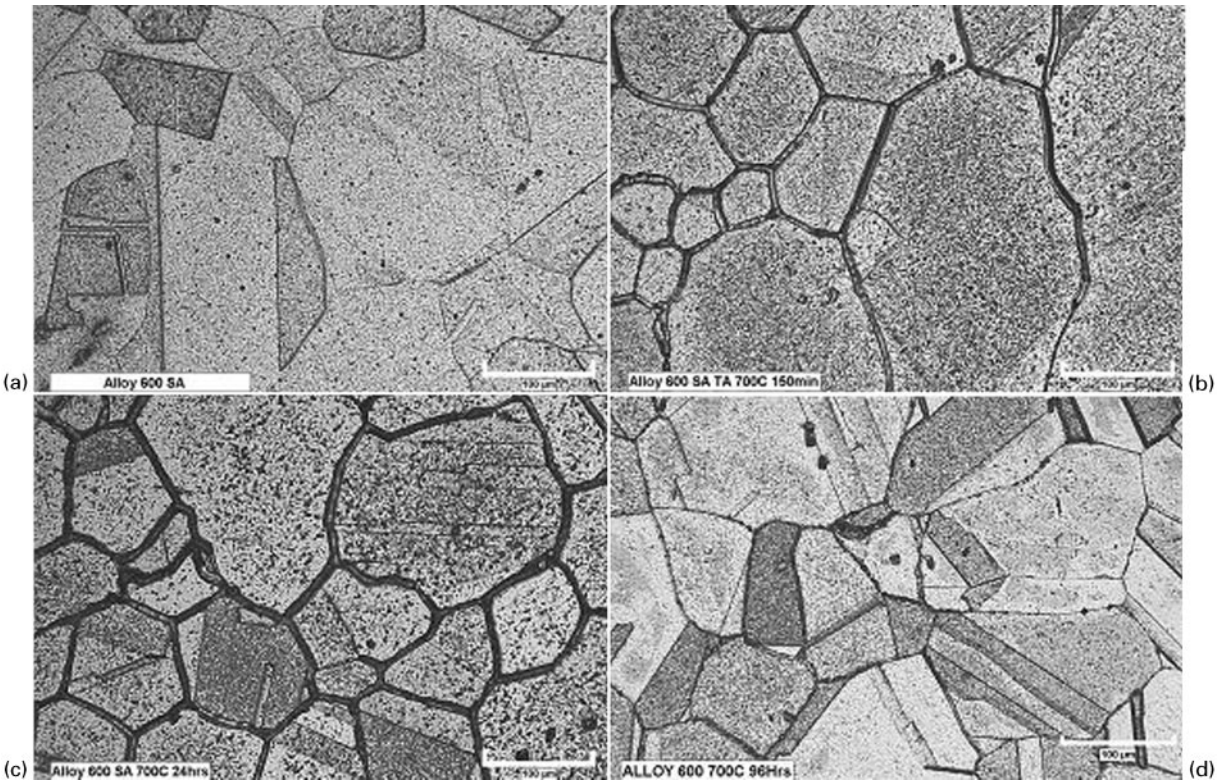

a solution annealed; *b* 2·5 h; *c* 24 h; *d* 96 h

6 Micrographs of EPR tested specimens

According to the trend in Fig. 5, alloy 600 materials with a C content of 0·02 should reach maximum sensitisation after 20 h, while materials with a C content of 0·04 should fully sensitise within 7 h. These predicted values are consistent with the results observed in Fig. 4. Additional support to verify sensitisation levels comes from examination of the exposed surface of the material following the EPR test. Sensitised areas along the grain boundaries (and eventually, within the grains) are preferentially corroded during the test and evident visually as furrows. Figure 6 shows the corroded microstructure for aged specimens from lot 1 tested with EPR.

The micrographs show increasing furrowing along the grain boundaries to 24 h and drastic reduction in furrowing after 96 h aging, information consistent with APR values (Fig. 4).

Cyclic potentiodynamic polarisation

Cyclic potentiodynamic polarisation was performed at 10^{-4}, 5×10^{-3} and 10^{-3}M Cl^-. The recorded repassivation potentials are shown as a function of chloride concentration for thermally aged specimens from lot 1 in Fig. 7.

An inverse relationship between repassivation potential and chloride concentration was observed. This was expected, as increasing Cl^- concentrations are more corrosive to 'stainless' alloys such as 600, even in the solution annealed state. Conflicting trends of E_{rcrev} with thermal aging treatments were observed at the varying concentrations. At 10^{-4}M Cl^-, the E_{rcrev} increased with thermal aging time, which suggests the alloy becomes more resistant to localised corrosion with sensitisation. At 10^{-3}M Cl^-, no observable trend was noted with aging time, and at 5×10^{-3}M Cl^-, an initial drop in E_{rcrev} is noted up to 10 h aging, after which the values return to the levels seen in the solution annealed condition. Further examination considers the charge density passed from each specimen during the repassivation scan. Previous studies have shown that for shallow pits, measured E_{rcrev} is dependent upon the charge density obtained during the test.[35] Figure 8 shows the

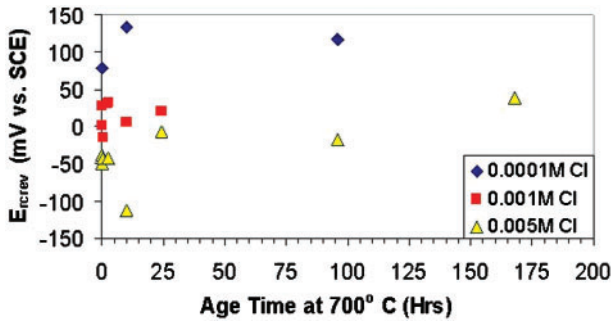

7 E_{rcrev} as function of Cl^- concentration measured with CPP

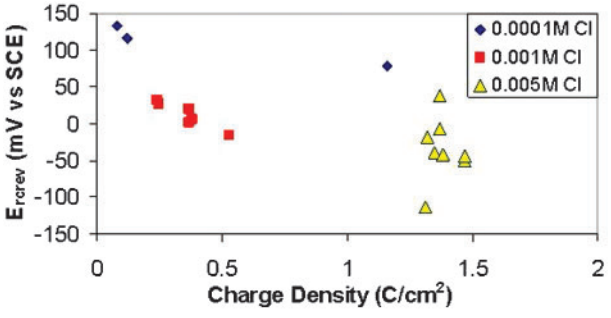

8 Dependence of measured E_{rcrev} on charge density passed during CPP scans at varying chloride concentrations for specimens aged at 700°C from 0 to 168 h

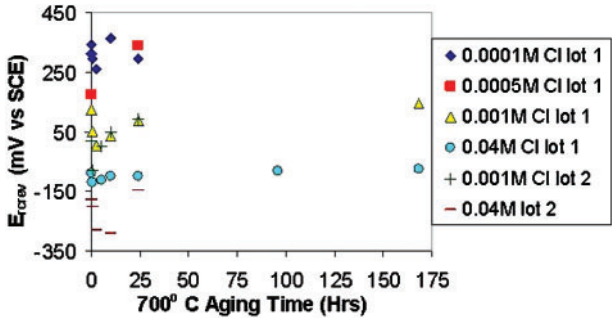

9 E_{rcrev} versus chloride concentration for alloy 600 measured with PS technique

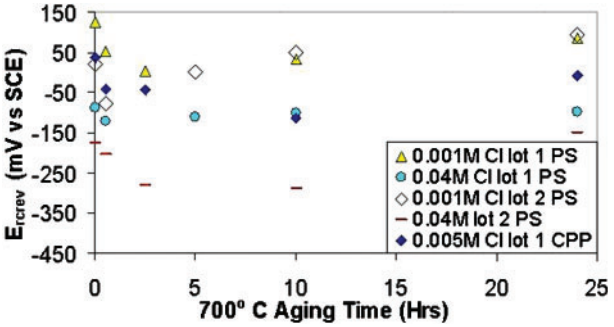

11 Dependence of E_{rcrev} on thermal aging treatment up to 24 h for measured values that were independent of charge density invoked during test

measured E_{rcrev} versus current density at each chloride concentration for all CPP scans.

At chloride concentrations 10^{-4} and 10^{-3}M, a strong inverse dependence of the measured repassivation potential on charge density is seen. This suggests that the trends seen for E_{rcrev} versus thermal aging treatment were confounded with the charge density, and not representative of sensitisation. However, at 5×10^{-3}M Cl^-, the measured E_{rcrev} is independent of the charge density passed, and the trend seen in Fig. 7, which correlated with that seen for EPR, may be attributed solely to sensitisation.

Potential staircase method

Scans using PS were performed for 10^{-4}M, 5×10^{-4}M, 10^{-3}M and 0·04M chloride concentrations. Plots showing the repassivation potential as a function of chloride concentration and aging time for lot 1 specimens are shown in Fig. 9.

Scans at 10^{-3} and 0·04M Cl^- concentrations showed trends in E_{rcrev} that loosely correlated with EPR and 5×10^{-3}M CPP E_{rcrev} data, while scans at 10^{-4}M and 5×10^{-4}M Cl^- concentrations did not. To better understand this discrepancy, Fig. 10 illustrates the charge density dependence of the measured E_{rcrev} values from Fig. 9 collectively in order to indicate which values were influenced by thermal aging, and which were dependent on the charge density.

A strong dependence of the measured repassivation potential on the charge density can be seen for charge densities $<2{\cdot}5$ C cm^{-2}. The strong dependence on charge density is especially relevant to the 10^{-4} and 5×10^{-4}M chloride concentrations, which are less corrosive and more difficult to initiate crevice corrosion. From Fig. 10, it can be concluded that the E_{rcrev} tests performed at 10^{-4} and 5×10^{-4}M Cl^- did not promote enough localised corrosion to yield E_{rcrev} measurements independent of the charge density invoked during the test.

Assuming that the measurements made at 10^{-3} and 0·04M Cl^- with the PS method, and at 5×10^{-3}M Cl^- with the CPP method are independent of current density, the trends seen in repassivation potential with aging time must be due to metallurgical effects. The individual values from these experiments may then be examined, shown collectively in Fig. 11, for repassivation potential measurements of lot 1 material.

The figure demonstrates that initial aging of the material is accompanied by a measured drop in the repassivation potential, but this drop was healed within 24 h thermal aging for most specimens. Lot 1 at 0·04M Cl^- showed the initial E_{rcrev} drop which was sustained for the entire 24 h (no healing).

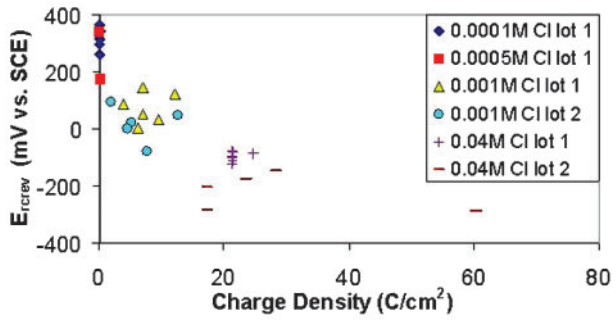

10 Dependence of measured repassivation potential on charge density for PS scans at varying chloride concentrations

Nitrate inhibited repassivation potentials

In addition to the effect of metallurgical condition, the effect of mixing nitrate inhibitor ions along with the chloride ions on E_{rcrev} was examined. The measured E_{rcrev} values are shown in Fig. 12 for solutions containing 0·04M Cl^-. The addition of nitrate increases the measured E_{rcrev} value, and seems to negate the influence of thermal aging condition on E_{rcrev}.

Discussion

Intergranular corrosion versus pitting/crevice corrosion

Intergranular corrosion occurs more or less uniformly across the whole specimen surface, if grain boundary precipitation is uniformly distributed. If the test

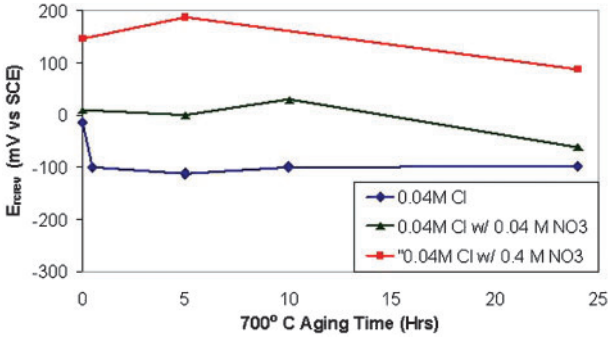

12 Effect of nitrate additions on repassivation potential of alloy 600

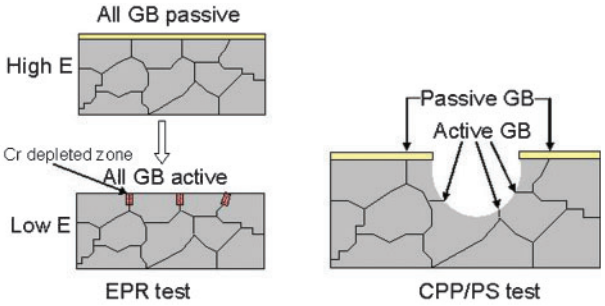

13 Schematic diagrams of EPR and CPP/PS (E_{rcrev}) test methods to illustrate differences in grain boundary effects

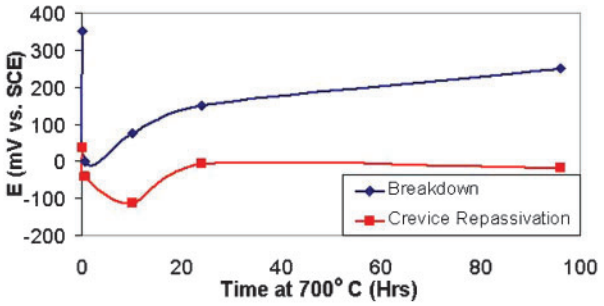

15 Comparison of E_{rcrev} and break-down potential from CPP scans of sensitised lot 1 material in 5×10^{-3}M Cl^-

environment is chosen appropriately, the measured parameter that indicates susceptibility to intergranular corrosion is then reflective of only the Cr depleted areas. Thus, the solution consisting of 0·05M $H_2SO_4+5\times10^{-5}$M KSCN at room temperature clearly differentiated between Cr depleted and non-depleted areas because the non-depleted alloy was passive in the solution. On the other hand, the higher sulphuric acid concentration resulted in even the non-depleted alloy exhibiting large active–passive transition. However, once an appropriately differentiating environment is chosen, the measured parameter shows the effect of all Cr depleted areas of the exposed surface. A second major characteristic of the intergranular corrosion test is that the rate of corrosion of the Cr depleted region is much higher (*see* Fig. 3) than the non-depleted region and, thus, the test measures kinetic differences between sensitised and non-sensitised material. Schematics shown in Fig. 13 provide further illustration of the difference between intergranular corrosion testing performed with EPR, and pitting or crevice corrosion testing performed with CPP and PS.

Typically, the dimensions of the pits before repassivation in these tests range from a hundred micrometres to 1 mm depending on the charge density. These sizes are considerably larger than the depletion size in this alloy, which is of the order of nanometers. Therefore, the E_{rcrev} measurements reflect the average of several grain boundaries and grain interiors. This is discussed in detail in a companion paper on modelling the thermal treatment effects.[29] Furthermore, the rate of corrosion inside a pit or active crevice region is not significantly different between a Cr depleted and non-depleted material because the corrosion occurs in a completely active state in a highly acidic environment. As we saw with the intergranular corrosion test in higher concentration H_2SO_4, the environment is too severe to distinguish between the rates of corrosion of depleted and non-depleted alloy. Therefore, because such a measurement is averaged over both grain boundary depleted and matrix non-depleted areas, qualitatively one might expect the recovery of the E_{rcrev} to be faster than that of the EPR values. This is consistent with the results shown in Fig. 14 where the recovery time for E_{rcrev} is faster than that for EPR.

Since the E_{rcrev} values are measured after considerable pit growth has occurred, one may suppose that the volume of damage has an influence on the measured effect of thermal treatment. The changes in the break-down and repassivation potentials, E_{crev} and E_{rcrev} respectively, from CPP scans of lot 1 material in 5×10^{-3}M Cl^- are plotted against thermal aging times in Fig. 15. It can be seen that the break-down potential, which is measured at an earlier stage of localised corrosion process, shows a decrease at lower aging times and a faster recovery.

As the concentration of the aggressive species in the solution (e.g. chloride) increases, the chromium threshold for oxide film formation increases as well, i.e. for a given chromium concentration, the active dissolution rate will increase slightly. But the effect is not as significant because the chloride concentration inside the pit is significantly higher than that of the external solution. Figure 16 shows that for both lots of alloy 600, higher chloride concentrations lead to longer recovery

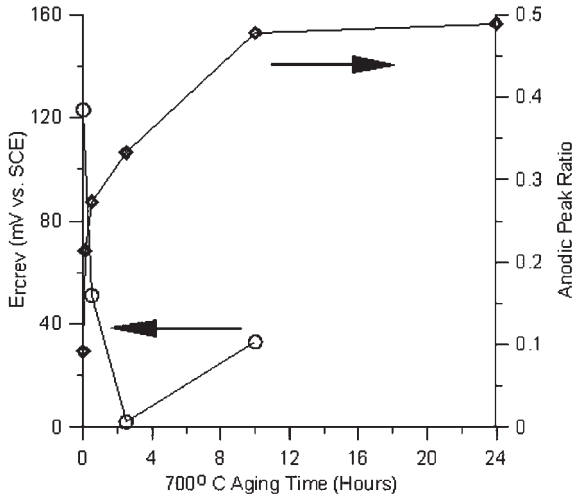

14 Comparison of sensitisation kinetics apparent from EPR and E_{rcrev} test results for lot 1 material (0·02C)

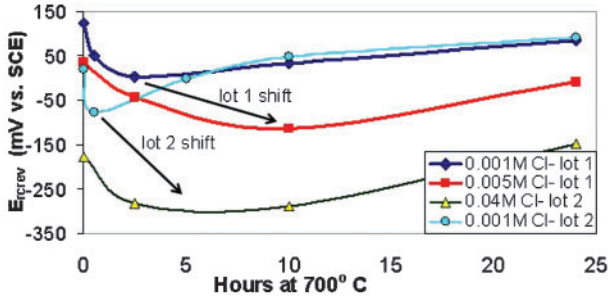

16 Shift in apparent sensitisation kinetics with chloride concentration when measuring E_{rcrev}

time. For the 0·02C content (lot 1) in a 10^{-3}M Cl^- solution, the minimum in E_{rcrev} occurs at 700°C for 2·5 h, whereas in a 5×10^{-3}M Cl^- solution, the material aged for 10 h is the most susceptible. For the 0·04C content (lot 2) in 10^{-3}M Cl^- solution, material aged for 0·5 h at 700° C is the most susceptible to localised corrosion, while at 0·04M Cl^-, material aged over 5 h is the most susceptible to localised attack. It is interesting to note that the value of E_{rcrev} is lower for the higher C alloy, although the decrease due to thermal treatment is not significantly different between the two carbon contents.

Dependence of E_{rcrev} on inhibitive species

Following the qualitative arguments above, if inhibitors that increase the oxide film forming rate are added, one may not expect any dependence of E_{rcrev} on thermal treatment. Figure 12 illustrates the relationship between E_{rcrev} and aging time for different inhibitor ion concentration for alloy 600. The data are again consistent with expectations.

Conclusions

1. Metallurgical influences on E_{rcrev} for thermally aged alloy 600 were determined. Thermal aging of these alloys results in carbide precipitation at grain boundaries, and a susceptibility to intergranular corrosion is expected. A 100–150 mV drop in measured E_{rcrev} was observed for initial aging times at 700°C for alloy 600, with healing observed within 24 h aging for all solutions tested.

2. Electrochemical potentiokinetic reactivation tests with 0·05M H_2SO_4 and 5E-5M KSCN solutions performed at room temperature were able to discern between various degrees of sensitisation for alloy 600, and tracked well with literature results for depletion volumes.

3. Kinetics for evolution of susceptibility to intergranular attack (sensitisation) apparent from both E_{rcrev} and EPR tests did not correlate. It is believed the different corrosivity of the test solutions, as well as the different aims of each test, resulted in this discrepancy. While EPR is valuable in ranking materials with respect to IGA susceptibility, it is too aggressive to predict the localised corrosion dependent lifetime expectancy of in service real world materials. E_{rcrev} was able to discern between different levels of sensitisation, and has been shown previously to be a better predictor for lifetime expectancy.

4. The effects of solution chemistry and temperature on E_{rcrev} were measured for alloy 600. Increasing chloride concentration and temperature resulted in decreasing E_{rcrev} as expected. The effects of nitrate additions to solution chemistry for thermally aged specimens of alloy 600 were measured. The inhibitor ions were found to offset the metallurgical influences on measured E_{rcrev}, and no GBCD influenced behaviour was noted for inhibitor added solutions.

Acknowledgements

The work reported here has been supported by the US Department of Energy (award number DE-FC36-04GO14043) and co-sponsored by ChevronTexaco, DuPont, Haynes International, Mitsubishi Chemical, Shell, and Toyo Engineering. The authors would like to acknowledge Mr Brian Derby and Mr John Duck at SwRI for technical expertise in implementing this study. In addition, we would like to thank Mr James F. Dante and Mr Darrell Dunn at SwRI for stimulating conversations regarding the nuances of both EPR and E_{rcrev} testing.

References

1. D. S. Dunn, Y.-M. Pan, L. Yang and G. A. Cragnolino: *Corrosion*, 2006, **62**, (1), 3–12.
2. M. H. Brown: *Corrosion*, 1969, **25**, (10), 438–443.
3. F. Duffaut, J.-P. Pouzet and P. Lacombe: *Corros. Sci.*, 1966, **6**, 83–85.
4. T. Yukitoshi, K. Yoshikawa and Y. Okada: Unpublished research, Sumitome Metal Industries Ltd, 1979.
5. G. S. Was, H. H. Tischner and R. M. Latanision: *Metall. Mater. Trans. A*, 1981, **12A**, 1397–1408.
6. E. L. Hall and C. L. Briant: *Metall. Trans. A*, 1985, **16A**, 1225–1235.
7. G. P. Airey, A. R. Vaia, N. Pessall and R. G. Aspden: *J. Met.*, 1981, **33**, 28–34.
8. R. C. Scarberry, S. C. Pearman and J. R. Crum: *Corrosion*, 1976, **32**, (10), 401–406.
9. I. L.W. Wilson, F. W. Pement, R. G. Aspden and R. T. Begley: *Nucl. Technol.*, 1976, **31**, 70–84.
10. I. L.W. Wilson and R. G. Aspden: *Corrosion*, 1976, **32**, 193–201.
11. G. P. Airey: *Corrosion*, 1979, **35**, (3), 129–136.
12. J. R. Cels: *Corrosion*, 1978, **34**, (6), 198–209.
13. G. P. Airey: *Corrosion*, 1979, **35**, (3), 129–136.
14. G. P. Airey: *Corrosion*, 1980, **36**, (1), 9–17.
15. R. Bandy, R. Roberge and R. C. Newman: *Corrosion*, 1983, **39**, (2), 391–398.
16. R. C. Newman, R. Roberge and R. Bandy: *Corrosion*, 1983, **39**, (2), 386–390.
17. R. Bandy and R. van Rooyen: *Corrosion*, 1984. **40**, (6), 281–289.
18. G. J. Theus: *Corrosion*, 1977, **33**, (1), 20–26.
19. H. A. Domian, R. H. Emanuelson, L. W. Sarver, G. J. Theus, and L. Katz: *Corrosion*, 1977, **33**, (1), 26–37.
20. R. S. Pathania: *Corrosion*, 1978, **34**, (5), 149–156.
21. A. R. McIlree and H. T. Michels: *Corrosion*, 1977, **33**, 60–67.
22. G. J. Theus: *Nucl. Technol.*, 1976, **28**, 388–397.
23. J. R. Weeks: in 'Corrosion problems in energy conversion and generation', (ed. J. C. S. Tedmon); 1974, Princeton, NJ, The Electrochemical Society.
24. G. P. Airey and F. W. Pement: *Corrosion*, 1983, **39**, (2), 46–55.
25. 'Standard practices for detecting susceptibility to intergranular attack in austenitic stainless steels', 262-02A, ASTM, Philadelphia, PA, USA, 2002.
26. A. Anderko, N. Sridhar and D. S. Dunn: *Corros. Sci.*, 2004, **46**, 1583–1612.
27. C. S. Brossia, N. Sridhar and A. Anderko: Proc. Conf. Eurocorr 2004, Paper 172, Nice, France, September 2004, NACE.
28. M. A. Jakab and A. Anderko: 'Prediction of corrosion of advanced materials and fabricated components', Final report, Department of Energy Project DE-FC36-04GO14043, S29, OLI Systems, Inc., Morris Plains, NJ, USA, 2007.
29. A. Anderko, N. Sridhar and G. Tormoen: *Corros. Eng. Sci. Technol.*, in press.
30. 'Standard test method for electrochemical reactivation (EPR) for detecting sensitization of AISI type 304 and 304L stainless steels', G108-94, ASTM, Philadelphia, PA, USA, 1994.
31. A. Mignone, A. Borello and A. La Barbera: *Corrosion*, 1982, **38**, (7), 390–402.
32. N. Sridhar, C. S. Brossia, D. S. Dunn and A. Anderko: *Corrosion*, 2004, **60**, (10), 915–936.
33. N. Sridhar and G. A. Cragnolino: *Corrosion*, 1993, **49**, (11), 885–894.
34. A. Anderko, N. Sridhar, M. A. Jakab and G. Tormoen: in press.
35. N. Sridhar and G. A. Cragnolino: *Corrosion*, 1993, **49**, (11), 885–894.